City Research Online

City St George's, University of London

Citation: Andriotis, A., Gavaises, M. & Arcoumanis, C. (2008). Vortex flow and cavitation in diesel injector nozzles. Journal of Fluid Mechanics, 610, pp. 195-215. doi: 10.1017/s0022112008002668

This is the unspecified version of the paper.

This version of the publication may differ from the final published version. To cite this item please consult the publisher's version.

Permanent repository link: https://openaccess.city.ac.uk/id/eprint/583/

Link to published version: https://doi.org/10.1017/s0022112008002668

Copyright and Reuse: Copyright and Moral Rights remain with the author(s) and/or copyright holders. Copies of full items can be used for personal research or study, educational, or not-for-profit purposes without prior permission or charge, unless otherwise indicated, provided that the authors, title and full bibliographic details are credited, a hyperlink and/or URL is given for the original metadata page and the content is not changed in any way. For full details of reuse please refer to City Research Online policy.

City Research Online: http://openaccess.city.ac.uk/ publications@citystgeorges.ac.uk

J. Fluid Mech. (2008), *vol.* 610, *pp.* 195–215. © 2008 Cambridge University Press
doi:10.1017/S0022112008002668 Printed in the United Kingdom

Vortex flow and cavitation in diesel injector nozzles

A. ANDRIOTIS, M. GAVAISES† AND C. ARCOUMANIS

Research Centre for Energy and the Environment, School of Engineering and Mathematical Sciences, City University, London, Northampton Square, EC1V 0HB London, UK

(Received 31 August 2007 and in revised form 29 May 2008)

Flow visualization as well as three-dimensional cavitating flow simulations have been employed for characterizing the formation of cavitation inside transparent replicas of fuel injector valves used in low-speed two-stroke diesel engines. The designs tested have incorporated five-hole nozzles with cylindrical as well as tapered holes operating at different fixed needle lift positions. High-speed images have revealed the formation of an unsteady vapour structure upstream of the injection holes inside the nozzle volume, which is referred to as 'string-cavitation'. Computation of the flow distribution and combination with three-dimensional reconstruction of the location of the strings inside the nozzle volume has revealed that strings are found at the core of recirculation zones; they originate either from pre-existing cavitation sites forming at sharp corners inside the nozzle where the pressure falls below the vapour pressure of the flowing liquid, or even from suction of outside air downstream of the hole exit. Processing of the acquired images has allowed estimation of the mean location and probability of appearance of the cavitating strings in the three-dimensional space as a function of needle lift, cavitation and Reynolds number. The frequency of appearance of the strings has been correlated with the Strouhal number of the vortices developing inside the sac volume; the latter has been found to be a function of needle lift and hole shape. The presence of strings has significantly affected the flow conditions at the nozzle exit, influencing the injected spray. The cavitation structures formed inside the injection holes are significantly altered by the presence of cavitation strings and are jointly responsible for up to 10 % variation in the instantaneous fuel injection quantity. Extrapolation using model predictions for real-size injectors operating at realistic injection pressures indicates that cavitation strings are expected to appear within the time scales of typical injection events, implying significant hole-to-hole and cycle-to-cycle variations during the corresponding spray development.

1. Introduction

The realization that diesel injector nozzles may cavitate under typical operating conditions inevitably adds a degree of complexity to the system design since, until recently, it was not clear how and when cavitation is formed and most importantly whether it has a beneficial influence on the exiting spray and the subsequent auto-ignition process. Relevant publications on the subject of cavitation in real-size diesel injectors are those of Chaves *et al.* (1995), Chaves & Obermeier (1998), Badock *et al.* (1999), Arcoumanis *et al.* (2000), while a number of studies have examined

† Author to whom correspondence should be addressed: m.gavaises@city.ac.uk

the development of cavitation in simplified transparent nozzle replicas, for example He & Ruiz (1995), Soteriou, Andrews & Smith (1995), Kim, Nishida & Hiroyasu (1997), Soteriou *et al.* (2001). Despite the significant amount of work, there is still uncertainty surrounding the advantages offered by the random formation of cavitation in enhancing the two-phase flow mixture at the exit of the nozzle and the effect this may have on possible wear of the nozzle metal body, as discussed by Gavaises *et al.* (2007). One approach gaining some support tries to eliminate cavitation completely through appropriate design of the hole entry and non-cylindrical shape of the holes (Blessing *et al.* 2003; Soteriou *et al.* 2006). Irrespective of the prevailing trend in nozzle design, thorough understanding of the nozzle internal flow is a prerequisite for designing the next generation of diesel engines for passenger cars, commercial and marine applications. Cavitation in such nozzles has been identified in two distinct forms according to Arcoumanis & Gavaises (1998) and Roth, Gavaises & Arcoumanis (2002). The geometric-induced cavitation is a relatively well-known phenomenon initiating at sharp corners where the pressure may fall below the vapour pressure of the flowing liquid. A second form of cavitation has been observed, and referred to as 'string' or 'vortex' cavitation by Afzal *et al.* (1999) and Roth *et al.* (2002). These two-phase flow structures are usually found in the bulk of the liquid, in the areas where large-scale, relative to the nozzle geometry, vortices exist. Although more recent studies have shown similar behaviour in various types of multi-hole nozzles, for example Nouri *et al.* (2007), their formation process has been found to be relatively irregular while their interaction with the mean flow remains poorly understood. Other studies on cavitation performed in venturi-type nozzles, for example see Gopalan, Katz & Knio (1999) and Gopalan & Katz (2000), have employed laser diagnostics to provide insight into the mechanism of bubble entrapment into vortical flow structures, but the complexity of the geometry of diesel injectors makes it difficul to obtain such measurements. Furthermore, because of the difficulty in obtaining real-time measurements during the injection process, most of the reported experimental studies refer to experimental devices simulating operating conditions relevant to those of diesel engines. Nevertheless, simplifications to the design of the nozzle itself or to the transient operation of the needle are unavoidable, which has implications on the very short injection durations and the very high liquid velocities, of the order of $400\,\mathrm{m\,s^{-1}}$ in production injectors. Parallel to the continuing effort to obtain better experimental information under as realistic conditions as possible, there is an increasing demand for developing and validating computational fluid dynamics models to predict cavitation. An increasing number of numerical models have appeared over the years in the literature which allow the formation and development of cavitation inside the nozzle to be simulated (Kubota, Kato & Yamaguchi 1992; Avva, Singhal & Gibson 1995; Schmidt, Rutland & Corradini 1997; Alajbegovic, Grogger & Philipp 1999; Marcer *et al.* 2000; Sauer, Winkler & Schnerr 2000; Singhal *et al.* 2001, 2002). Each model is based on different assumptions while various numerical methodologies have been used for implementation in commercial or in-house fluid-flow solvers. Most models are based on the assumption that cavitation is a mechanically driven phenomenon initiated by the presence of nuclei which grow to become bubbles and then form the complex cavitation structures observed experimentally. Despite the effort devoted to developing cavitation models applicable for fuel injectors, all of those applied so far have focused on geometric-induced cavitation. It can be argued that there is no model yet capable of predicting string cavitation in fuel-injection equipment. This is mainly due to the lack of experimental data available for the relevant flow phenomena and, thus, the incomplete physical understanding of the process. As it will be revealed later

in this paper, the aforementioned models are, in principle, incapable of simulating string cavitation inside injector nozzles. Some studies on vortex cavitation, for example Chahine & Duraiswami (1992) and Chahine & Kalumuck (2002), which represent a promising theoretical background to this problem, have not yet been applied to nozzle flows.

The present paper represents an extension to Gavaises & Andriotis (2006) and aims to provide new experimental data for the origin, formation, development, lifetime and influence on the nozzle hole flow of vortex-type or string cavitation. The designs investigated include multi-hole injectors used in low-speed two-stroke diesel engines. The specific design of these nozzles allows for clear optical access to all holes and the nozzle sac volume to be obtained. In addition, their relatively large size compared to that of automotive injectors offers the possibility of obtaining images of cavitation in a 1:1 scale. This has been achieved by manufacturing a number of fully transparent acrylic nozzle replicas, which have allowed optical access into the nozzle volume upstream of the injection holes, inside them as well as into the sprays formed at the nozzle exit. The designs tested include a number of cylindrical as well as tapered (converging) holes; the latter greatly modify the pressure distribution at the hole entry and may prevent formation of geometric cavitation, thus, providing evidence about the origin of string cavitation in the absence of hole cavitation. Use of two synchronised high-speed cameras has allowed reconstruction of the location of the cavitation strings inside the three-dimensional nozzle sac volume as well as characterization of the frequency of their appearance and development, as a function of the needle lift, cavitation and Reynolds number. Use of computational fluid dynamics (CFD) models has provided information about the local flow field at the location where cavitation strings start developing. Image collection over long enough times has provided information about their lifetime and an estimate of the mean volume they occupy inside the nozzle tip. At the same time, measurements of the flow rate both in the absence and in the presence of cavitation strings has provided information about their effect on the flow-rate variation between individual injection holes. These measurements have been combined with flow imaging of the cavitation structures inside the injection holes. As expected, the hole flow is influenced by the co-existence and interaction of the geometric-induced cavitation, which is normally always present, and the relatively unsteady string cavitation. In turn, simultaneous imaging of the flow inside the nozzle holes and the near nozzle spray formation has shown that the atomization process of the injected liquid is greatly affected by the cavitation strings. This results not only in uneven liquid dispersion within the significantly increased spray cone angle, but also in hole-to-hole variations.

The next section of the paper describes the experimental set-up used, followed by a brief description of the CFD model employed for simulating the single-phase internal nozzle flow as well as the cavitation formation and development inside the injection holes. Then the various results obtained are presented, followed by the most important findings which are summarized at the end.

2. Experimental set-up and test cases

Various transparent five-hole nozzles were manufactured from a transparent acrylic material; the nozzle geometry is shown in figure 1. All holes are concentrated on one 90° sector; this is because of the size of the engine they operate which has a bore diameter of about 1.0 m. Three fuel valves are installed on the engine cylinder head which inject the fuel circumferentially – rather than in the radial direction as

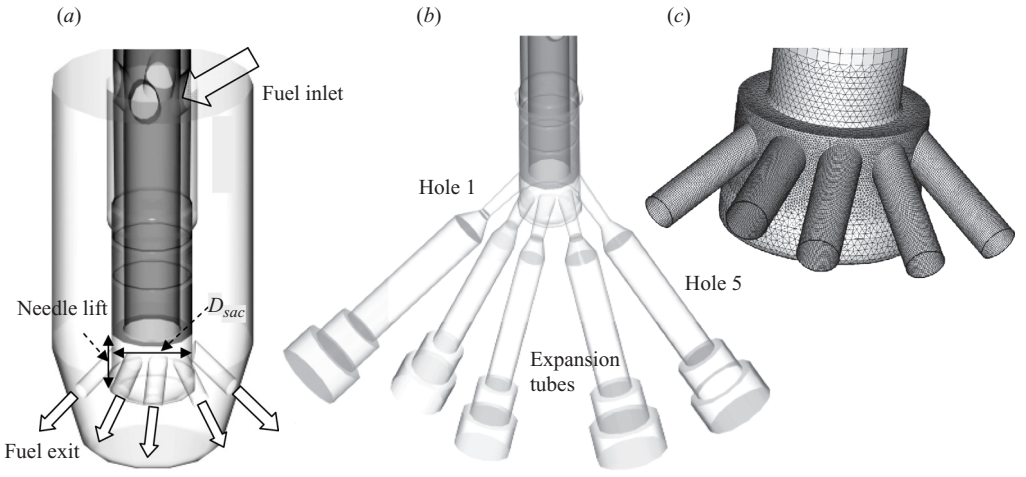

FIGURE 1. Nozzle geometries investigated (*a*) 5-hole nozzle without expansion tubes, (*b*) 5-hole nozzle with expansion tubes and (*c*) unstructured computational grid for the 5-hole nozzle with local refinement upstream and at the entry to the injection holes.

in passenger car diesel engines. Another important characteristic of this nozzle is the shape of the needle. As can be seen in figure 1, there is a hollow slide-type needle which seals the injection holes directly, leaving almost zero sac volume when it closes. When the needle opens, the slide uncovers the injection holes and fuel flows from the fuel line in the inner part of the hollow needle, allowing fuel injection. The volume below the needle and upstream of the injection holes will be referred to as 'nozzle volume', and it is equivalent to the 'sac volume' of passenger car diesel injectors. The transparent nozzle of figure 1(*a*) is manufactured on a 1:1 scale and it injects liquid directly into ambient air under room temperature and atmospheric pressure; the working fluid is water at 25 °C. This nozzle was used for visualization of the liquid atomization process which also allowed at the same time visualization of the cavitation strings. The nozzle of figure 1(*b*) was enlarged to a 2:1 scale and it was used for investigating the internal nozzle flow in more detail; specially designed discharge channels were manufactured for allowing injection into liquid without restricting the nozzle hole flow upstream. In this way, splashing of the liquid on the outer surfaces of the injector was prevented and thus, clear images of the internal nozzle flow have been obtained. Two different versions of nozzles have been manufactured, one with cylindrical and one with tapered holes. The nominal injection hole exit diameter for both real-size nozzle designs is about 1.5 mm while the tapered holes incorporate a 4° full cone angle; the needle lift at its full (stop) position is about 3.7 mm.

The test rig used has been used in a number of studies and it is described in detail by Roth *et al.* (2002). The flow rate was controlled by a valve in the pipe downstream of the feed pump and measured by an ultrasonic flow meter. The flow rate from each of the injection holes was also measured simultaneously with the incoming flow rate. Both the injection pressure and the pressure downstream of the injection holes were adjusted by restricting the inflow and outflow of the injector, respectively. In order to reach sub-atmospheric back pressures corresponding to higher cavitation numbers, a suction pump was installed in addition to the main feed pump. The Reynolds number has been defined on the basis of the mean flow rate and the average hole diameter while the cavitation number is defined here as

Flow rate ($l\,s^{-1}$)	Feed pressure (bar)	Back pressure (bar)	Cavitation number	Reynolds number
0.13	1	0.5	0.5	10 000
0.9	6	1.3	5	68 000

TABLE 1. Range of operating conditions investigated.

$CN = (P_{INJ} - P_{BACK})/(P_{BACK} - P_{VAPOUR})$, where P_{INJ}, P_{BACK} and P_{VAPOUR} represent the injection, ambient and vapour pressures, respectively. Since the fuel flow through the injector nozzles, especially through the holes, is highly turbulent, all flow features are expected to behave transiently and within short time scales. Since it is important to gain knowledge about the dynamics of cavitation inception and formation processes for various flow conditions, two high-speed digital video systems were set up and synchronized in order to capture the cavitating structures from two perpendicular views. Correlation of the obtained images with the numerical grid used for the CFD analysis has allowed reconstruction of the instantaneous location and volume of the strings inside the nozzle. Temporal averaging of sufficient number of strings has provided the probability of finding a cavitation string at a specific location inside the nozzle volume for different operating conditions. Alternatively, superposition of images obtained from the bottom view only has allowed the temporal and spatial averaging of the string location over the whole nozzle volume depth. This has provided a relatively easy way for comparing different cases where the cavitation strings form at different locations within the nozzle volume in relation to the different injection holes. It has to be noted that although imaging from the bottom view can capture the flow structure in all 5 holes and the nozzle volume simultaneously, imaging from the side view is restricted to only hole 1 or hole 5, depending on the positioning of the camera. The Photron FASTCAM-ultima APX cameras used here are able to take up to 120 000 frames per second (f.p.s.) with an exposure time as low as 4 ns and a maximum resolution of 1024×1024 at 3000 f.p.s. For the particular cases investigated here, usually 6000 to 16 000 f.p.s. were sufficient to capture the temporal development of cavitation using a shutter time of 30 μs. In total, up to 4000 images were collected for a particular case. A strong halogen floodlight together with some halogen spotlights were necessary to provide enough light for the intensified CCD video chip in combination with the high frame rates. The operating conditions tested are summarized in table 1; they refer to cavitation numbers between 0.5 and 5, which are similar to those of production injectors operating under engine operating conditions. However, the much lower injection pressures used here restrict the experiment into flow rates (and Reynolds number) much lower than those of the real operating conditions. Imaging was performed for various combinations of the listed parameters and for different needle lifts. The values to be reported here correspond to the 'full' or 'nominal' lift, which corresponds to the nominal stop position of the needle in the real injector. The 'low' lift case corresponds to a needle lift at about 80 % of the full one. In this case, the slide is just uncovering the injection holes. Finally, the 'high' lift case corresponds to 120 % of the full lift position.

3. Numerical model

The in-house GFS RANS flow solver, as modified by Giannadakis (2005), has been used to simulate the flow inside the nozzles tested. This model is able to simulate the

geometric-induced hole cavitation, but not string cavitation; thus, model predictions can be used only complementarily to the experimental results, in order to assist in the interpretation of the obtained images. For the liquid phase, the volume and ensemble averaged continuity and Navier–Stokes equations are solved. As a result of the dynamic interaction of the cavitation bubbles with the surrounding pressure field, the available volume for the liquid phase can change significantly. The effect of the additional vapour is taken into account by including the liquid phase volume fraction α_l (referred to as liquid fraction) in the conservation equations. Moreover, owing to the slip velocity between the cavitation bubbles and the flowing liquid, there is additional interaction which is taken into account with the inclusion of the appropriate source terms in the conservation equations:

$$\frac{\partial}{\partial \mathrm{t}}(\alpha_L \rho_L) + \nabla \cdot (\alpha_L \rho_L \boldsymbol{u}_L) = 0, \tag{1}$$

$$\frac{\partial(\alpha_L \rho_L \boldsymbol{u}_L)}{\partial t} + \nabla \cdot (\alpha_L \rho_L \boldsymbol{u}_L \otimes \boldsymbol{u}_L) = -\nabla p + \alpha_L \nabla \cdot ((\mu_L + \mu_t)(\nabla \otimes \boldsymbol{u}_L + (\nabla \otimes \boldsymbol{u}_L)^T)) + s_{momentum}, \tag{2}$$

where μ_t is the eddy viscosity, calculated by

$$\mu_t = C_\mu \rho_L \frac{k_L^2}{\varepsilon_L}. \tag{3}$$

In (2), with the term $s_{momentum}$ the effect of the cavitation bubbles' relative motion upon the liquid phase is taken into account. Although a model that can address the combined effect of turbulence and cavitation on the flow has as yet not appeared, nozzle flows are highly turbulent, the standard two-equation k–ε has been employed for the consideration of turbulence effects. The additional effect of the bubbles' relative movement on the liquid phase turbulent kinetic energy and dissipation are also included according to the approach of Laín *et al.* (2002). Note that as part of the numerous numerical tests that have been performed during the development of the model, a number of other turbulence models have been tested, apart from the standard k–ε, namely the RNG of Yakhot *et al.* (1992) and the non-equilibrium version of Shyy *et al.* (1997) as applied in the simulation of cavitating flows by Vaidyanathan *et al.* (2003). Overall, it can be claimed that although a variation of up to 3 % in the predicted nozzle discharge coefficient can be attributed to the turbulence model Giannadakis *et al.* (2007), the details of the underlining physical processes are not affected significantly; furthermore, no model has been found to persistently predict cavitation better than the rest for all test cases, within the context of the Reynolds-averaged methodology. For this reason, it is believed that the model adopted here represents a robust engineering tool for the current state of the model's sophistication. The SIMPLE algorithm of Patankar & Spalding (1972) is used to solve for the continuous phase flow field. In single-phase calculations of nozzle flows with injection and back pressures corresponding to cavitation numbers high enough for cavitation to be present, the location of its inception is identified from the numerical cells where the pressure falls below vapour pressure. The volume of all the Eulerian grid cells where pressure is below vapour is referred to as 'tension volume' and it provides a quantitative indication of how much liquid is stretched owing to the flow. Cavitation initiates and then further develops by the existence of small spherical bubble nuclei assumed to pre-exist within the liquid, following a pre-assigned size and number distribution according to Meyer, Billet & Holl (1992). The model is based on the Eulerian–Lagrangian approach, while the liquid phase is

modelled as the continuous phase and the cavitation bubbles as the dispersed one. Many of the fundamental physical processes assumed to take place in cavitating flows are incorporated into the model. These include bubble formation through nucleation, momentum exchange between the bubbly and the carrier liquid phase, bubble growth and collapse due to nonlinear dynamics according to the early study of Prosperetti & Plesset (1978), bubble turbulent dispersion as proposed by Farrell (2003) and bubble turbulent/hydrodynamic breakup, based on the experimental observations of Martínez-Bazán, Montañés & Lasheras (1999). The effect of bubble coalescence and bubble-to-bubble interaction on the momentum exchange and during bubble growth/collapse is also considered. More details and a thorough validation of the model can be found in Giannadakis (2005) and Giannadakis *et al.* (2007).

All simulations performed are transient even for fixed geometry and boundary conditions; the second-order Crank–Nicolson discretization scheme has been employed for modelling the time derivatives of the solved equations. The time step used for the simulation of the nozzle volume flow has been varied between 10^{-4} to 10^{-5} s, which is short enough to capture the transient development of the vortices formed inside the nozzle. However, a much shorter time step of 0.5×10^{-7}s has been used for simulating the cavitation structures formed inside the injection hole; note that an adaptive time step with values down to 10^{-12} s is used in the integration of the Rayleigh–Plesset equation proposed by Plesset & Prosperetti (1977), for simulating the growth and collapse of the cavitation bubbles. Regarding spatial discretization, the second-order scheme of Papadakis & Bergeles (1995) has been used in addition to the first-order hybrid one. Fully unstructured numerical grids consisting of tetrahedral and hexahedral elements have been used. The number of computational cells has been varied between 65 000 and 600 000 for the nozzle volume while ~50 000 cells have been used inside each of the injection holes. That corresponds to an average cell size of ~0.4 to 0.075 mm, which has been considered small enough to resolve the large-scale vortices forming inside the nozzle volume. Finally, in addition to the low-pressure transparent nozzles tested and simulated, predictions have also been obtained for injection pressures up to 600 bar, which is the nominal pressure of the injectors under investigation that allowed useful conclusions to be drawn for the operation of these nozzles.

4. Results and discussion

A general description of the flow distribution inside the nozzles tested is given first, including experimental images of the cavitation structures formed inside the nozzle volume and the injection holes, as well as CFD predictions for the nozzle volume flow pattern. Although flow images can be obtained only at low injection pressures relative to those used in real injectors, it can be argued that the conclusions to be drawn are valid also for the actual conditions. Evidence to support this is based not only on past studies comparing cavitation in large-scale and real-size nozzles as reported by Arcoumanis *et al.* (2000) and Roth *et al.* (2005), but also on model predictions to be reported here.

A number of questions may be raised regarding the dynamics of cavitation strings, and, in particular, the location where they develop, how do they form and what effect do they have on the nozzle flow and the injected spray. These three questions will be addressed in the following sections.

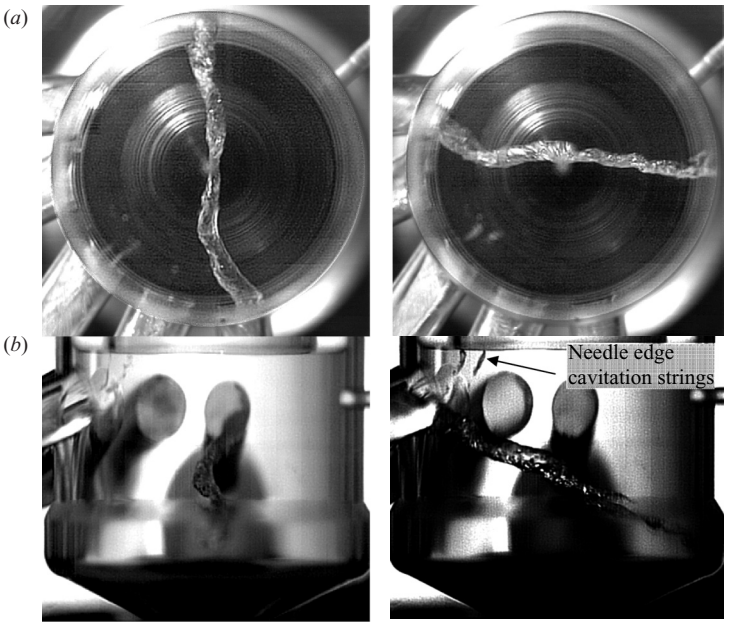

FIGURE 2. Typical image of string cavitation formed inside the nozzle volume at two different time instances with $\Delta\tau \sim 100$ (*a*) bottom view and (*b*) side view (nominal needle lift, $CN = 4.0$, $Re = 68\,000$).

4.1. *Flow structure*

The presentation of the results starts from a general description of the flow distribution inside the specific nozzles investigated. Figure 2 shows typical images of the string cavitation formed inside the nozzle volume at a nominal needle lift, $CN = 4$ and $Re = 68\,000$, at two time instances with $\Delta\tau \sim 100$; $\tau = t/t^*$ is the non-dimensional time introduced here, where the normalization time scale used is equal to $t^* = D_{SAC}/U_{SAC}$; U_{SAC} is the mean axial velocity entering into the sac (nozzle) volume and D_{SAC} is the diameter of the nozzle (figure 1*a*); with this scaling approach, it will be possible to compare the vortex development inside the sac volume for different operating flow rates through the nozzle. Images are presented from both the bottom and the side views. It can be seen that well inside the nozzle volume, a relatively thick and long vapour structure is formed; this two-phase flow structure will be referred to from now as 'string cavitation'.

Figure 3(*a*, *b*) shows the predicted flow paths inside the nozzle volume upstream as well as inside the injection holes obtained for the nominal needle lift case at two different times with $\Delta\tau \sim 100$; It can be seen that as the flow enters from upstream into the nozzle volume, it turns around 90° in order to exit from the nozzle holes. As a result, a strong recirculation zone is formed inside the nozzle volume; the presence of this vortex is rather important for the subsequent analysis. Time-dependent predictions have revealed that for specific operating conditions this vortex may be rather unstable and move inside the nozzle volume. The streamlines plotted show that this vortex is connected in the first instance to hole 5 and in the second to hole 1. This instability in the location of the vortex will be further analysed later on in this section. Irrespective of the vortex motion upstream of the injection holes, as the flow enters through the sharp corner entry hole, the pressure may drop locally below the

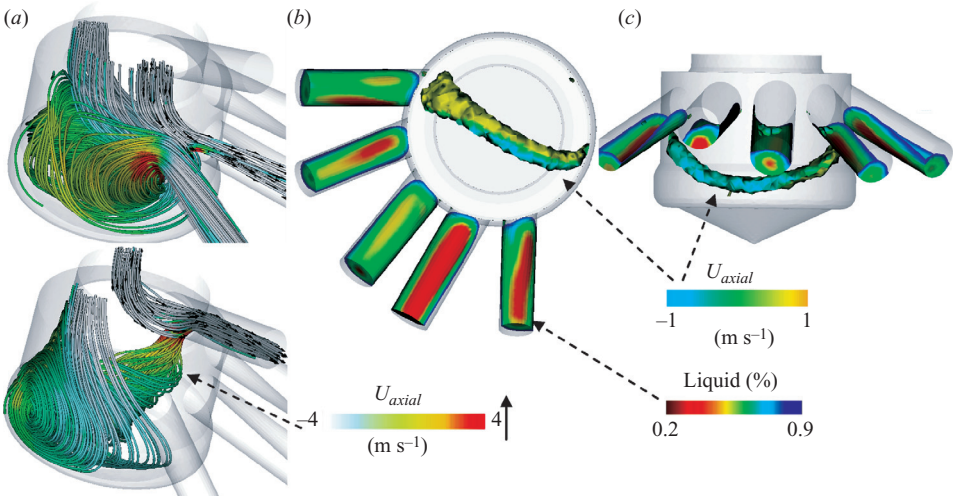

FIGURE 3. Prediction of flow structure inside the sac volume (*a*) path lines of vortex in front of hole 1, (*b*) vortical structure at $\Delta\tau \sim 100$ relative to previous flow, showing the vortical structure located in front of hole 5 and (*c*) predicted cavitation vapour volume fraction iso-surfaces inside the nozzle holes and core of the nozzle volume vortex coloured with the axial velocity component of the incoming liquid, as seen from two different views (nominal needle lift, $CN = 4.0$, $Re = 68\,000$).

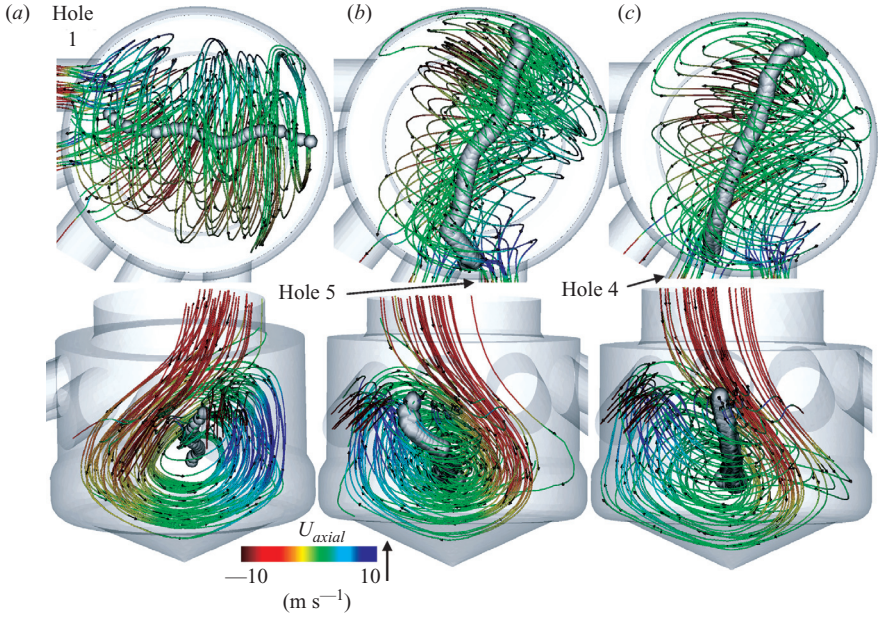

FIGURE 4. Three-dimensional reconstruction of the visuallized string cavitation superimposed on the calculated flow field (*a*) nominal lift, string connected to hole 1 and (*b*) nominal lift, string connected to hole 5 with $\Delta\tau \approx 100$ and (*c*) low needle lift case, string connected to hole 4 ($CN = 4.0$, $Re = 68\,000$).

vapour pressure of the flowing liquid, which initiates cavitation. Since each hole has a different orientation relative to the nozzle, cavitation initiates at a different location relative to the corresponding hole entry and develops inside in a rather asymmetric

three-dimensional shape. Figure 3(*c*) shows two views of an instantaneous cavitation pattern as predicted by the model in all five holes, together with the predicted core of the nozzle volume vortex. The core of the vortex can be identified from the iso-surfaces of the swirl intensity, which is a parameter frequently used to locate and track vortical flow structures according to Jeong & Hussain (1995); here the selected iso-surface is coloured with the axial velocity component of the incoming liquid in order to highlight the change in the direction of the flow. It can be argued that hole cavitation itself is a rather transient phenomenon, but the time scales of the relevant processes are a few orders of magnitude smaller than the development of the vortical structure observed inside the nozzle volume. The macroscopic structure of the two-phase flow formed inside the injection holes is mainly a function of the cavitation number. Measurements of the nozzle discharge coefficient reported by Gavaises & Andriotis (2006) as a function of the cavitation number for different Reynolds numbers have revealed that the overall volumetric flow rate of the nozzle is a function of only the cavitation number for a fixed needle lift, and not of the Reynolds number. In agreement with previously reported data of Arcoumanis *et al.* (1999), when cavitation initiates, the nozzle discharge coefficient drops and reaches asymptotically a minimum value for a fully developed cavitating flow.

4.2. *String cavitation location*

Following the general description of the flow distribution inside the nozzle, it is appropriate to proceed towards the presentation of the observed cavitation strings. As shown in figure 2, in this area, model predictions indicate that the pressure of the flowing liquid is almost equal to the feed pressure and much greater than the vapour pressure of the liquid. Despite that, string cavitation has been identified as developing in a transient mode. The location of the string seems to change considerably, since it may be connected to either hole 1 or hole 5, as the images taken at different time instances reveal, and to correlate well with the vortical structures formed inside the nozzle volume. Proof of that is provided in figure 4(*a*, *b*) where the CCD images, which have been obtained simultaneously from two perpendicular views (bottom and side), have been used to reconstruct the string in the three-dimensional space inside the nozzle volume. The long string was then discretized into a sufficient number of vapour pockets along the string centreline and with radius equal to that of the actual string. Those experimental or 'virtual' vapour pockets, which have the same total volume as the actual string, could be numerically handled as numerical bubbles and inserted into the numerical grid only for visualization purposes, but not for actual multi-phase flow calculations in this area. As the results indicate, the observed cavitation strings are formed at the core of the large-scale recirculation zones developing transiently inside the nozzle volume.

Figure 4(*c*) shows a similar set of predictions and cavitation string reconstruction, but this time for the low needle lift case where the string is connected to hole 4 only and not to holes 1 or 5, as for the nominal needle lift case; it can thus be expected that the position of the needle affects the formation of the recirculation zones formed inside the nozzle.

Having identified the location of the cavitation strings inside the nozzle volume, we can proceed to the presentation of various cases aiming to identify the effect of geometric and operating parameters on the string cavitation structure. Since cavitation strings develop in a highly transient mode and are not always present at the same operating condition (e.g. during the image collection process a significant number of them are string-cavitation-free), it was considered useful to derive mean images.

From the reconstruction, not only can the string location be correlated with the local flow field, but also their volume can be estimated. The simpler approach is to derive a mean image only from the bottom view images. Temporal and spatial averaging includes not only the time steps where string cavitation is present, but also those where it is absent. Since the raw images provide only a projection of the string on the camera plane, the averaged image effectively corresponds to a mean projected view rather than to a full three-dimensional representation; this approach has proved useful in comparing different cases. Figure 5, also reported in Gavaises & Andriotis (2006), presents three sets of results corresponding to the initial development of both hole and string cavitation for the low needle lift case. At low cavitation numbers, around 0.5, no string is evident and only hole 3 starts to cavitate. With a slight increase of the cavitation number to about 0.6, all holes start to cavitate, but not continuously, while a string appears to develop inside the nozzle volume and exits mainly from hole 4. Since the maximum level of the mean image corresponds to about 20 % according to the attached scale, and since the observed string is only present more or less in the same location and exits always from hole 4, it can be deduced that string cavitation is actually formed during only 20 % of the time of the whole flow process. A further increase in the cavitation and Reynolds numbers results in a higher probability of string formation. At the same time, hole cavitation seems to become well established in all holes, reaching the exit of holes 3 and 4, but within holes 1, 2 and 5 it disappears before reaching the exit. For cavitation numbers above 0.9, all holes cavitate continuously. The six images of figure 6, obtained at $Re = 53\,000$, show that the two-string pattern is always present while the probability value slightly increases with increasing cavitation number. Cavitation structures also seem to be present in front of all holes; these are smaller cavitation structures appearing at the space between the sharp edge of the needle and the hole inlet, as indicated on the CCD image of figure 2. Since cavitation strings have been linked with the vortical structures attached to pre-existing cavitation sites, in an effort to induce string cavitation patterns at different locations inside the sac volume, some holes have been blocked. Corresponding results are shown in figure 7 for the nominal needle lift case. Blocking of the flow through hole 2 results in the co-existence of two cavitation strings (figure 7*a*). In addition to the large cavitation structure in front of hole 4, a smaller string connecting holes 1 and 3 is formed; such a pattern has been previously observed with automotive diesel injectors, as reported for example by Afzal *et al.* (1999) and Roth *et al.* (2002). Since in figure 7(*a*) the string is attached to hole 4, this hole was then additionally blocked. The image of figure 7(*b*) reveals now that the string is attached to hole 3 while the shorter vortex connecting this hole with hole 1 has disappeared. Proceeding in a similar manner, blocking of hole 3 results in the formation of string cavitation in front of hole 5 only. It is thus evident that by modifying the flow distribution within the sac volume the formation of cavitation strings also follows the resulting vortical flow pattern. Although not included here, simulation of the location of the vortex inside the nozzle under these conditions, matches well with the observed cavitation patterns.

In addition to the two-dimensional (bottom view) mean projected image, the following three-dimensional temporal and spatial averaging has been performed. From the three-dimensional reconstruction of the instantaneous string location the volume occupied by its outer surface has been estimated. Spatial and temporal averaging of a sufficient number of strings has allowed estimation of the probability of finding a string present in the three-dimensional space. A typical result from this process is shown in figures 8(*a*) and 8(*b*) for the low lift and the full needle

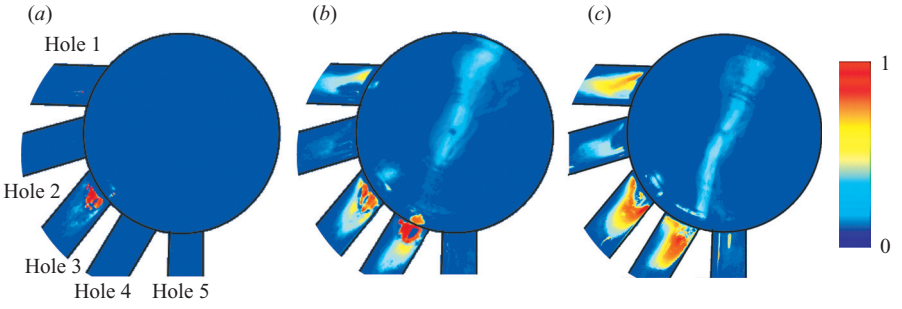

FIGURE 5. Effect of increasing flow rate on two-dimensional temporally and spatially averaged images of string cavitation probability, showing the initial stages of the development of hole and string cavitation (*a*) $CN = 0.5$; $Re = 31\,000$, (*b*) 0.6; 35 000, (*c*) 0.7; 39 000 (from Gavaises & Andriotis 2006).

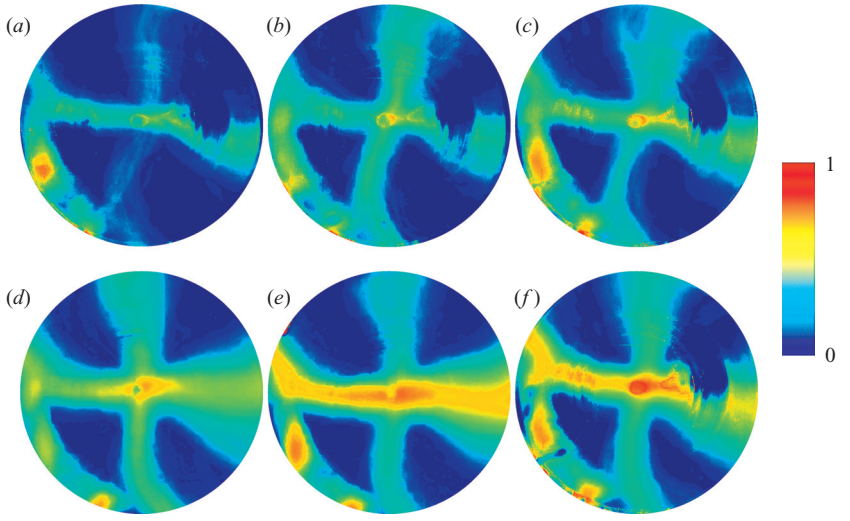

FIGURE 6. Effect of cavitation number on two-dimensional temporally and spatially averaged images of cavitation string probability (nominal needle lift, $Re = 53\,000$ (*a*) $CN = 0.9$; (*b*) 1.0, (*c*) 1.2, (*d*) 2.6, (*e*) 3.0, (*f*) 4.25.

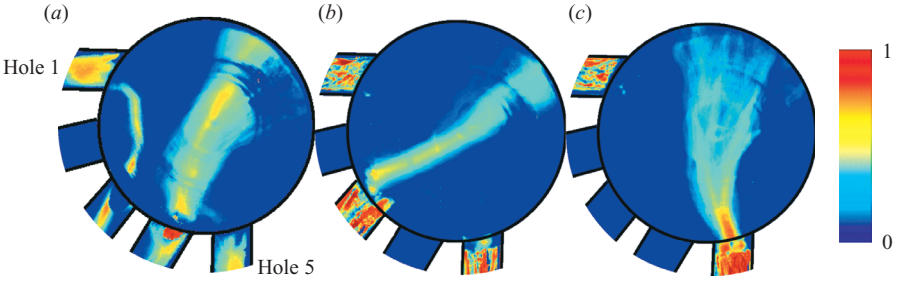

FIGURE 7. Two-dimensional spatially averaged images of cavitation string probability or different scenarios of hole combination blocking: (*a*) hole 2 blocked, (*b*) hole 2 and 4 blocked and (*c*) holes 2, 3 and 4 blocked (nominal needle lift, $CN = 2.6$, $Re = 45\,000$)

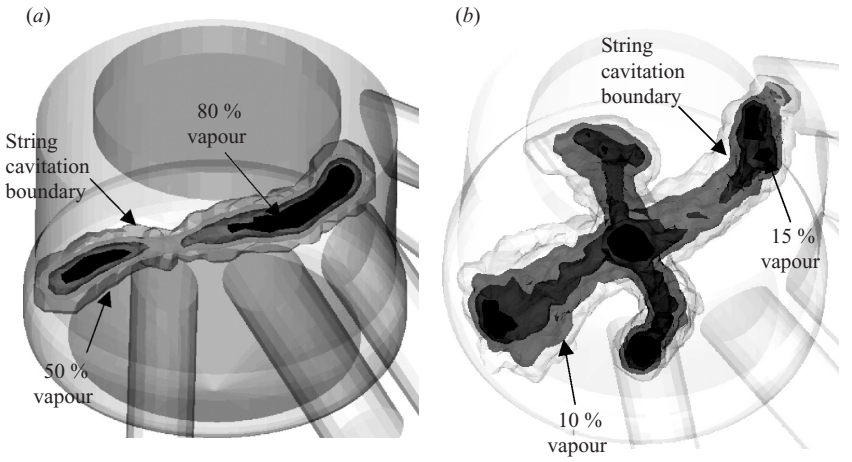

FIGURE 8. Three-dimensional iso-surfaces of cavitation string cavitation probability for (*a*) low lift and (*b*) nominal lift ($CN = 2.0$, $Re = 39\,000$).

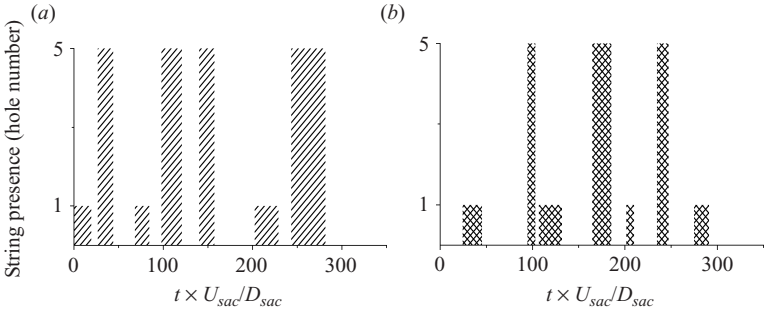

FIGURE 9. Comparison between (*a*) measured temporal evolution of string cavitation presence next to holes 1 and 5 and (*b*) predicted vortex core presence attached to these holes (nominal needle lift, $CN = 5.0$, $Re = 68\,000$).

lift cases, respectively. On these plots, three iso-probability surfaces are plotted. The first one depicts the most remote location that strings may reach as they transiently move inside the nozzle volume. The second iso-surface value plotted for the low needle lift case (figure 8*a*), where strings have been found to be continuously present, corresponds to the boundary where strings are present 50 % of their lifetime. Finally, the last one on the same figure shows the iso-surface of 80 % vapour, which can be interpreted as the volume always occupied by cavitation strings. For the nominal needle lift case, strings are observed for less than 50 % of the running time and they are attached either to hole 1 or hole 5 and never overlap with each other. This implies that the maximum calculated probability value should be less than 25 %; the 10 and 15 % iso-surfaces plotted in figure 8(*b*) reveal the string structure for this particular operating condition.

For the nominal needle lift case where the two-string structure has been identified, it was considered useful to register the time sequence of appearance of cavitation strings. Figure 9(*a*) presents the time history of the string presence for the nominal needle lift case. On these plots, three bar values are plotted on the *y*-axis, corresponding to string attached to hole 1, to hole 5 and no cavitation string. The *x*-axis corresponds

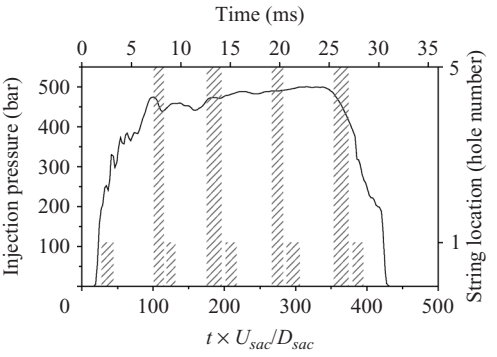

FIGURE 10. Input pressure boundary condition used for the simulation of the internal nozzle flow for the real-size injector operating under engine conditions with superimposed the predicted temporal evolution of the vortex presence in holes 1 and 5; the similarity with the large-scale nozzle presented in figure 9 is evident.

to the dimensionless time τ introduced previously. With this scaling, it is possible to identify the frequency of vortex formation inside the sac volume and, thus, the Strouhal number of the recorded periodic flow pattern. From the experimental results, it can be observed that there is no string overlapping period while the time interval between successive string appearances is almost the same as their lifetime; the latter is of the order of $\tau \approx 15$–20 for this particular operating condition. Cavitation strings reappear in front of the same injection hole about every $\tau \approx 70$–80. A similar set of predictions, this time for the presence of the vortex core in front of the corresponding injection hole are shown in figure 9(*b*). The core of the vortex can be identified from the iso-surfaces of the swirl intensity shown previously in figure 2(*d*); the iso-surface used has been selected in such a way as to have the same diameter as that of the observed strings near the inlet to the injection holes. Note the close similarity between the observations and model predictions. Model predictions reveal that the vortical structure formed inside the nozzle volume is moving with a low-speed circumferential velocity component relative to the nozzle axis. Cavitation strings appear when the core of the vortex is attached to an injection hole. The combined experimental finding for the string lifetime and the predicted flow pattern lead to the conclusion that cavitation strings appear when the nozzle volume vortex is attached to an injection hole. This is an important conclusion and will be further supported in the following section of the paper which investigates the origins of cavitation strings. Similar predictions for realistic operating conditions may provide evidence for the appearance of strings during engine operation (figure 10). On the same plot, the injection pressure profile used is shown; this pressure profile has been measured under engine operating conditions just upstream of the nozzle inlet. In figure 10, the predicted vortical structure presence in front of holes 1 and 5 is also plotted similarly to the previous figure. It is clear that model predictions suggest at least 3 events of string cavitation formation even for the much shorter injection event. The vortex develops during the same normalized time τ with almost the same frequency, thus the same Strouhal number; thus this scaling can be used to extrapolate results from the transparent but low flow rate nozzles to the actual injectors operating at much higher pressures. It ought to be mentioned here that similar computational results have been obtained for a wide range of parametric studies, not reported here, which have addressed the effect of spatial and temporal discretization methods, including

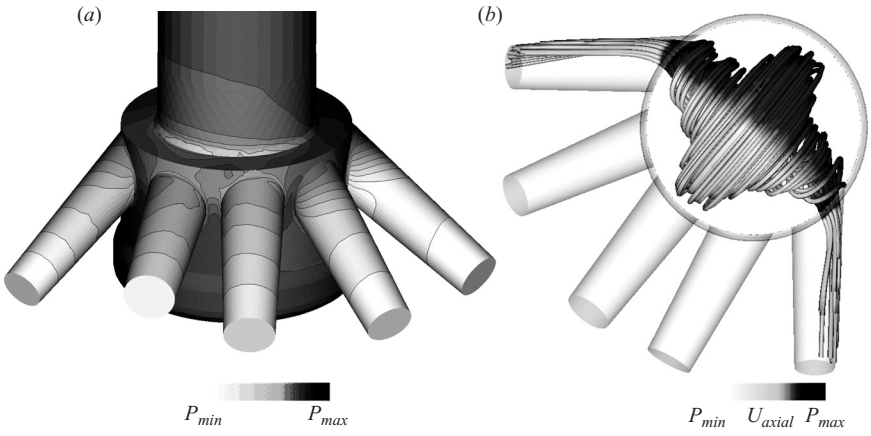

FIGURE 11. (*a*) Predicted pressure distribution inside the tapered large-scale 5-hole nozzle and (*b*) instantaneous image of the vortical structure formed inside the sac volume (high needle lift, $CN = 3.0$, $Re = 53\,000$).

first- and second-order ones, the effect of the time step which has been reduced down to two orders of magnitude, the effect of the number of computational cells which has been increased four times as well as the effect of different turbulence models, including different realizations of the k-ε model, the k-omega and the Reynolds stress one. Out of these studies, it has been safely concluded that model predictions are not sensitive to these parameters with respect to the formation and development of the nozzle vortical flow structures.

4.3. *Origin of cavitation strings*

The next set of results to be reported here refers to the origin of the cavitation strings. As already mentioned, the location of the string has been correlated with the core of the vortex formed inside the nozzle volume. Furthermore, it has been argued that one mechanism for the appearance of cavitation strings is associated not only with the existence of the vortex, but with its direct link with a cavitating site formed at the hole inlet. Formation of vortex cavitation as a result of the pressure drop within the core of the vortex has been abandoned as a mechanism on the basis of model predictions which indicate pressure levels much higher than the vapour pressure of the flowing liquid. In other words, combination of experimental observations and model predictions has indicated that cavitation strings form from pre-existing cavitation sites; if these come into contact with a vortex, then vapour may be trapped inside the vortex core and form the observed string cavitation structures with the high-speed camera. To further support this hypothesis, two transparent nozzles with tapered (converging) holes have been manufactured; the first nozzle incorporates expansion tubes and the second does not, while the rest of the geometry was identical to the nozzle with the cylindrical holes. Model predictions indicate that hole cavitation should not be expected for this nozzle since the pressure distribution at the hole inlet is greatly modified by the hole shape; conical holes create a much smoother pressure gradient (figure 11*a*) and do not cavitate even for much higher pressures relative to the cylindrical ones. This is a well-known characteristic for such nozzles which also exhibit a higher discharge coefficient, as reported by Soteriou *et al.* (2006). For this nozzle design, the flow distribution inside the nozzle volume is expected to be similar to that with cylindrical holes. Evidence of that was provided by the simulated flow

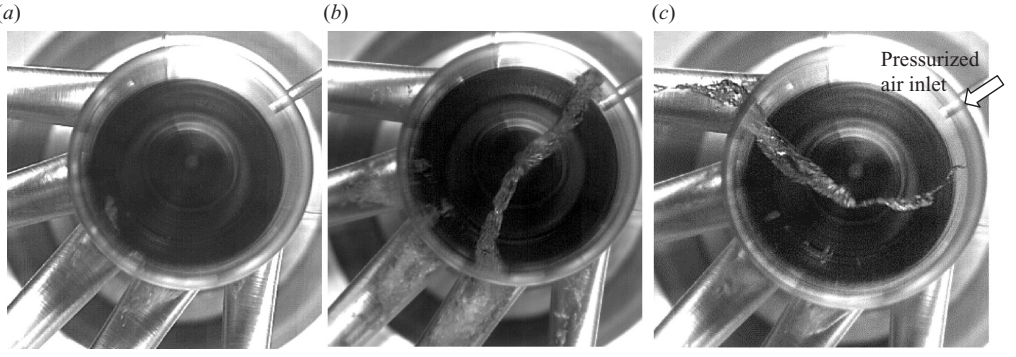

FIGURE 12. Representative image for the geometric hole cavitation-free tapered 5-hole nozzle with (*a*) absence of string cavitation at high needle lift, (*b*) presence of string cavitation next to hole 4 at low needle lift and (*c*) air bubbles introduced into the sac volume in the area of the vortex development at high needle lift, resulting to an induced string-like two-phase flow structure ($CN = 3.0$, $Re = 53\,000$).

field shown in figure 11(*b*). As can be seen, the vortical structure inside the nozzle is still present and follows a similar pattern of motion as in the previous nozzle for the same needle lift; however, some differences do exist and will be reported in the following section. Visualization of the flow inside the nozzle with the expansion tubes, which is the case for injection of liquid into liquid, has revealed that this design was string-cavitation free; a typical bottom-view CCD of this nozzle operating at the maximum Reynolds and cavitation numbers with the needle placed at its nominal lift can be seen in figure 12(*a*). This image also reveals the absence of hole cavitation except in hole 4, where there is some evidence of cavitation initiation and subsequent collapse within the injection hole before cavitation bubbles could reach the hole exit. As expected, for this particular needle lift, the nozzle vortex was not in contact with hole 4 and no string was observed. On the contrary, when the needle was placed at low lift which has been associated with a continuous presence of the vortex in front of this hole, a cavitation string has been observed to form in exactly the same manner as in the case of cylindrical holes; a typical image can be seen in figure 12(*b*). Further evidence of the realization that cavitation strings are simply carriers of liquid vapour or air trapped within recirculation zones is provided in figure 12(*c*). This image has been obtained at the same operating conditions as figure 12(*a*). This time, however, pressurized air bubbles have been artificially introduced into the flow from a pressure taping used to record the pressure inside the nozzle. When such bubbles are trapped in the vortex forming within the nozzle volume, their initially spherical shape could develop into the string-like structure observed in this image. It can thus be argued that the observed cavitation strings do not contain vapour produced at the core of the vortices, but rather vapour originating from pre-existing cavitation sites and trapped within the core of the vortices formed upstream of the injection holes.

It could be of interest to report results obtained from the tapered nozzle without the expansion tubes which represents the case of injection directly into ambient air. For the particular test case reported here, the nozzle has been operating at sufficiently high needle lift and low enough flow rate to prevent the formation of hole cavitation. Despite that, the side-view high-speed images shown in figure 13 reveal the formation of a string originating from the hole exit and developing upstream towards the hole inlet and then into the nozzle volume. This was an unexpected result never observed

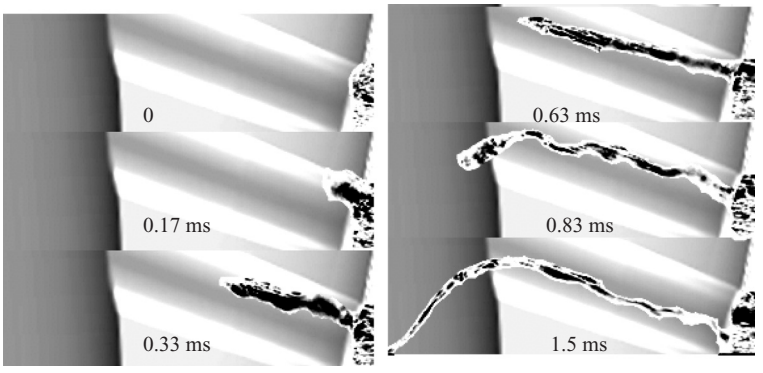

FIGURE 13. Sequence of high-speed images showing the formation of string cavitation originating at the nozzle exit and moving upstream inside the nozzle volume (nominal needle lift, $CN = 1.0$, $Re = 39\,000$).

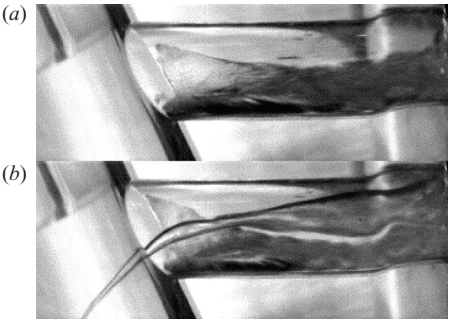

FIGURE 14. Effect of string cavitation on the flow distribution inside the injection hole, as seen from the side view (*a*) with string cavitation and (*b*) without string cavitation (nominal needle lift, $CN = 4.0$, $Re = 53\,000$).

in previous studies. Flow simulations indicate the presence of swirling flow inside the injection hole which could explain the formation of the observed string. The implications of this observation are that two-phase flow realized in a form similar to cavitation strings may be present with tapered holes even in the absence of nozzle hole cavitation sites.

4.4. *Effect of string cavitation on hole flow*

Having identified the mechanism leading to the formation of cavitation strings and their dependence on geometric parameters and operating conditions, it was considered important to investigate their effect on the hole flow structure. As already described, the geometric-induced cavitation is taking place in the injection holes, as both flow images and model predictions have indicated. It should be also recalled that hole cavitation was highly asymmetric and different from hole to hole, owing to the highly swirling motion of the flow entering through individual injection holes, as shown in figure 2(*d*).

Figure 14 shows a side view CCD image of the cavitating structures developing inside injection hole 1 in the absence and in the presence of a cavitation string. These images give a clear indication that once a cavitation string enters the injection hole, the two separate cavitation structures become indistinguishable and a much larger cavitation cloud dominates the flow; this extended cavitation cloud seems to occupy

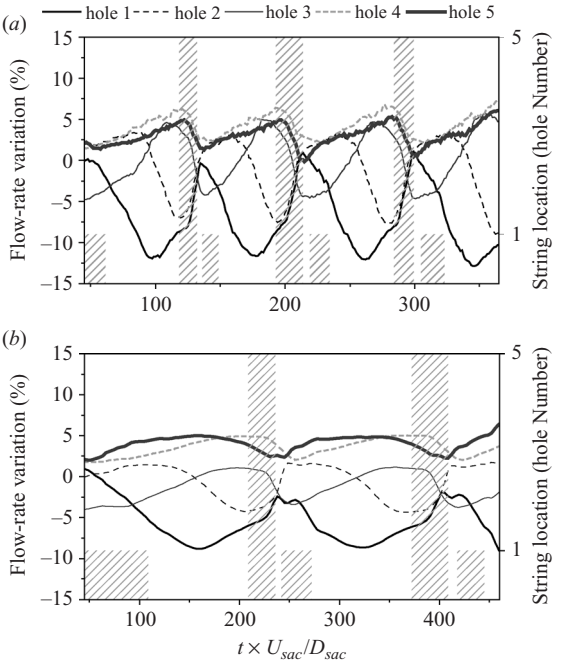

FIGURE 15. Predicted temporal variation of hole-to-hole flow rate for (*a*) cylindrical 5-hole nozzle and (*b*) tapered large-scale 5-hole nozzle (nominal needle lift $CN = 4.0$, $Re = 53\,000$).

the full cross-sectional area of the injection hole in the presence of string cavitation. As reported by Gavaises & Andriotis (2006), around 10 % reduction of the hole flow rate is associated with the presence of a cavitation string attached to an individual injection hole. However, in that study, it was not possible to distinguish from the experimental data whether this effect is related to the flow distribution upstream of the injection hole or is simply the effect of the increased vapour volume inside the injection hole in the presence of a cavitation string. Evidence of this can be provided by the CFD model. Figures 15(*a*) and 15(*b*) show the calculated instantaneous flow rate from each of the five injection holes for the cylindrical and the tapered nozzle holes, respectively. These predictions have been obtained with the needle at its nominal lift and within a time window during which the vortical structure changes its location from hole 1 to hole 5 for both cases simulated here. It is clear that hole 1 exhibits the highest flow-rate variation with flow rate peaking when the nozzle vortex is facing the opposite hole 5 and dropping when the vortex enters it. The maximum calculated reduction is ∼10 % in the case of the cylindrical holes and ∼8 % in the case of tapered holes; the average flow-rate reduction for the time window during which the nozzle flow vortex is attached to this particular hole is ∼5–7%. It can be thus concluded that the measured flow-rate reduction in the presence of a string can be attributed to the reduced liquid quantity entering the hole when the flow vortex is attached to it. The rest of the observed flow rate reduction can be attributed to the modified cavitating flow structure inside the injection hole in the presence of the increased cavitation vapour. Comparing the predicted temporal flow-rate variation between the cylindrical and the tapered holes, it can be concluded that the nozzle vortex switches from hole 1 to hole 5 faster for the case of the cylindrical holes, confirming that the nozzle flow development is sensitive not only to the needle lift, but also to the geometric

characteristics of the nozzle. Finally, it should be mentioned that the presence of strings has a significant effect on the formation of the injected sprays as reported by Andriotis, Spathopoulou & Gavaises (2007) and Andriotis & Gavaises (2009).

5. Conclusions

Cavitation formed in the nozzle of fuel injection equipment for passenger car and marine diesel engines has been identified as one of the main parameters affecting the nozzle discharge coefficient, the momentum of the injected liquid and the spray dispersion angle. The understanding of the flow mechanisms taking place in such nozzles is a prerequisite for the design of advanced systems which require accurate control to minimize spray-to-spray and shot-to-shot variations. Previous studies have categorized the observed cavitation structures forming inside injector nozzles as geometric-induced and dynamic-induced or string cavitation. Although adequate data exist for geometric-induced cavitation, limited information is available for the dynamic one. The present study has provided experimental data confirming the presence of string cavitation and addressing unresolved questions about its origin, area of formation, lifetime and influence on the nozzle hole flow. The visualization method employed has made simultaneous use of two high-speed cameras observing the two-phase flow structures forming inside transparent replicas of nozzles used in low-speed two-stroke diesel engines. Interpretation of the obtained images has been assisted by computational fluid dynamics predictions of the nozzle and hole flow. The specific designs tested included five-hole nozzles with cylindrical as well as tapered holes operating at different fixed needle lift positions; nevertheless, the conclusions drawn for the observed flow mechanisms can be extrapolated to other nozzle designs where string cavitation is also present. Images have revealed formation of an unsteady vapour structure upstream of the injection holes inside the nozzle volume, referred to as 'string cavitation'. From the images, it has been possible to reconstruct the location of the observed structures inside the nozzle volume. Combination of images with the simulated flow field has revealed that cavitation structures are found at the areas of flow circulation and they originate either from pre-existing cavitation sites forming at sharp corners inside the nozzle where the pressure falls below the vapour pressure of the flowing liquid, or even from suction of outside air downstream of the hole exit. This has been made possible by the manufacturing of nozzles with tapered holes which suppress the formation of geometric cavitation and thus have enabled data of string cavitation in controlled combination or in the absence of geometric cavitation to be obtained. Processing of the acquired images has allowed estimation of the mean location and probability of appearance of the cavitating strings inside the nozzle volume space, as a function of needle lift, cavitation and Reynolds numbers. The frequency of appearance of strings has been correlated with the Strouhal number of the large-scale vortices developing inside the nozzle volume; the latter has been found to be sensitive to the geometric characteristics of the nozzle, including the needle lift and the shape of the injection holes. Large variations in the instantaneous fuel injection quantity of individual injection holes have been recorded when a cavitation string is observed inside them. Combination with model predictions has revealed that the observed reduction in the individual hole flow rate is partially attributed to the increased vapour fraction inside the hole when a string is present; the vortex flow developing upstream of the hole entry is the main reason for the observed trend. Extrapolation based on model predictions for real-size injectors operating at realistic

injection pressure indicates that cavitation strings are expected to appear within the time scales of typical injection events.

REFERENCES

Afzal, H., Arcoumanis, C., Gavaises, M. & Kampanis, N. 1999 Internal flow in diesel injector nozzles: modelling and experiments. *IMechE Paper* S492/S2/99.

Alajbegovic, A., Grogger, H. A. & Philipp, H. 1999 Calculation of transient cavitation in nozzle using the two-fluid model. *Proc. 12th Annu. Conf. on Liquid Atomization and Spray Systems. Indianapolis, Indiana, USA.*

Andriotis, A. & Gavaises, M. 2009 Influence of vortex flow and cavitation on near-nozzle diesel spray dispersion angle. *Atomiz. Sprays* **19**, 1–24.

Andriotis, A., Spathopoulou, M. & Gavaises, M. 2007 Effect of nozzle flow and cavitation structures on spray development in Low-speed two-stroke diesel engines. *Proc. CIMAC 2007, Vienna, May 2007.*

Arcoumanis, C. & Gavaises, M. 1998 Cavitation in diesel injectors: modelling and experiments. *Proc. ILASS-EUROPE. Manchester, UK.*

Arcoumanis, C., Flora, H., Gavaises, M., Kampanis, N. & Horrocks, R. 1999 Investigation of cavitation in a vertical multi-hole injector. *SAE Trans. J. Engines* 1999-01-0524, **108-3**.

Arcoumanis, C., Badami, M., Flora, H. & Gavaises, M. 2000 Cavitation in real-size multi-hole diesel injector nozzles. *SAE Trans. J. Engines* 2000-01-1249 **109-3**.

Avva, R. K., Singhal, A. & Gibson, D. H. 1995. An enthalpy based model of cavitation. *Cavitation and Multiphase Flow Forum, ASME FED*, pp. 63–70.

Badock, C., Wirth, R., Fath, A. & Leipertz, A. 1999 Investigation of cavitation in real size diesel injection nozzles. *Intl J. Heat Fluid Flow* **20**, 538–544.

Blessing, M., König, G., Krüger, C., Michels, U. & Schwarz, V. 2003 Analysis of flow and cavitation phenomena in diesel injection nozzles and its effect on spray and mixture formation. SAE Paper 2003-01-1358.

Chahine, G. L. & Duraiswami, R. 1992 Dynamical interactions in a multi-bubble cloud. *Trans ASME J. Fluids Engng* **114**, 680–686.

Chahine, G. L. & Kalumuck, K. M. 2002 Simulation of surface piercing body coupled response to underwater bubble dynamics utilizing 3DYNAFS, a three-dimensional BEM Code. *Proc. IABEM 2002 – International Association for Boundary Element Methods. Austin, Texas, USA.*

Chaves, H. & Obermeier, F. 1998 Correlation between light absorption signals of cavitating nozzle flow within and outside of the hole of a transparent diesel injection nozzle. *Proc. ILASS-EUROPE. Manchester, UK.*

Chaves, H., Knapp, M., Kubitzek, A. & Obermeier, F. 1995. Experimental study of cavitation in the nozzle hole of diesel injectors using transparent nozzles. SAE Paper 950290.

Farrell, K. J. 2003. Eulerian/Lagrangian analysis for the prediction of cavitation inception. *Trans. ASME J. Fluids Engng* **125**, 46–52.

Gavaises, M. & Andriotis, A. 2006 Cavitation inside multi-hole injectors for large diesel engines and its effect on the near-nozzle spray structure. *SAE Trans. J. Engines* 2006-01-1114 **115-3**, 634–647.

Gavaises, M., Papoulias, D., Andriotis, A., Giannadakis, E. & Theodorakakos, A. 2007 Link between cavitation development and erosion damage in diesel fuel injector nozzles. *SAE Paper* 2007-01-0246.

Giannadakis, E. 2005. Modelling of cavitation in automotive fuel injector nozzles. PhD thesis, Imperial College, University of London.

Giannadakis, E., Papoulias, D., Gavaises, M., Arcoumanis, C., Soteriou, C. & Tang, W. 2007 Evaluation of the predictive capability of diesel nozzle cavitation models. *SAE Paper* 2007-01-0245

Gopalan, S. & Katz, J. 2000 Flow structure and modeling issues in the closure region of attached cavitation. *Phys. Fluids* **12**, 895–911.

Gopalan, S., Katz, J. & Knio, O. 1999 The flow structure in the near field of jets and its effect on cavitation inception. *J. Fluid Mech.* **98**, 1–43.

He, L. & Ruiz, F. 1995 Effect of cavitation on flow and turbulence in plain orifices for high-speed atomization. *Atomiz. Sprays* **5**, 569–584.

Jeong, J. & Hussain, F. 1995 On the identification of a vortex. *J. Fluid Mech.* **285**, 69–94.

Kim, J. H., Nishida, K. & Hiroyasu, H. 1997 Characteristics of internal flow in a diesel injection nozzle. *Proc. ICLASS. Seoul, Korea.*

Kubota, A., Kato, H. & Yamaguchi, H. 1992 A new modelling of cavitating flows–a numerical study of unsteady cavitation on a hydrofoil section. *J. Fluid Mech.* **240**, 59–96.

Laín, S., Bröder, D., Sommerfeld, M. & Göz, M. F. 2002 Modelling hydrodynamics and turbulence in a bubble column using the Euler–Lagrange procedure. *Intl J. Multiphase Flow* **28**, 1381–1407.

Marcer, R., Le Cottier, P., Chaves, H., Argueyrolles, B., Habchi, C. & Barbeau, B. 2000 A validated numerical simulation of diesel injector flow using a VOF method. *SAE Paper* 2000-01-2932.

Martínez-Bazán, C., Montañés, J. L. & Lasheras, J. C. 1999 On the breakup of an air bubble injected into a fully developed turbulent flow. Part 2. Size PDF of the resulting daughter bubbles. *J. Fluid Mech.* **401**, 183–207.

Meyer, R. S., Billet, M. L. & Holl, J. W. 1992 Freestream nuclei and traveling-bubble cavitation. *J. Fluids Engng. Trans ASME* **114**, 672–679.

Nouri, J. M., Mitroglou, N., You You Yan & Arcoumanis, C. 2007 Internal flow and cavitation in a multi-hole injector for gasoline direct-injection engines. *SAE Paper* 2007-01-1405.

Papadakis, G. & Bergeles, G. 1995 A locally modified 2nd-order upwind scheme for convection terms discretization. *Intl J. Numer. Meth. Heat Fluid Flow* **5**, 49–62.

Patankar, S. V. & Spalding, B. D. 1972 A calculation procedure for heat, mass and momentum transfer in three-dimensional parabolic flows. *Intl J. Heat Mass Transfer* **15**, 1787–1806.

Plesset, M. S. & Prosperetti, A. 1977 Bubble dynamics and cavitation. *Annu. Rev. Fluid Mech.* **9**, 145–185.

Prosperetti, A. & Plesset, M. S. 1978. Vapour-bubble growth in a superheated liquid. *J. Fluid Mech.* **85**, 349–368.

Roth, H., Gavaises, M. & Arcoumanis, C. 2002 Cavitation initiation, its development and link with flow turbulence in diesel injector nozzles. *SAE Trans. J. Engines*, 2002-01-0214 **111-3**, 561–580.

Roth, H., Giannadakis, E., Gavaises, M., Arcoumanis, C., Omae, K., Sakata, I., Nakamura, M. & Yanagihara, H. 2005 Effect of multi-injection strategy on cavitation development in diesel injector nozzle holes. *SAE Trans. J. Engines* 2005-02-1237 **114-3**, 1029–1045.

Sauer, J., Winkler, G. & Schnerr, G. H. 2000 Cavitation and condensation – common aspects of physical modeling and numerical approach. *Chem. Engng & Technol* **23**, 663–666.

Schmidt, D. P., Rutland, C. J. & Corradini, M. L. 1997 A numerical study of cavitating flow through various nozzle shapes. SAE Paper 971597.

Shyy, W., Thakur, S., Ouyang, H., Liu, J. & Blosch, E. 1997 *Computational Techniques for Complex Transport Phenomena.* Cambridge University Press.

Singhal, A. K., Athavale, M. M., Li, H. Y. & Jiang, Y. 2001 Mathematical basis and validation of the full cavitation model. *Proc. FEDSM'01 – 2001 ASME Fluid Engng Division Summer Meeting. New Orleans, Louisiana, USA.*

Singhal, A. K., Athavale, M. M., Li, H. Y. & Jiang, Y. 2002 Mathematical basis and validation of the full cavitation model. *Trans ASME J. Fluids Engng* **124**, 617–624.

Soteriou, C., Andrews, R. J. & Smith, M. 1995 Direct injection diesel sprays and the effect of cavitation and hydraulic flip on atomization. SAE Paper 950080.

Soteriou, C., Andrews, R. J., Torres, N., Smith, M. & Kunkulagunta, R. 2001 Through the diesel nozzle hole – a journey of discovery. *Proc. ILASS Americas, 14th Annu. Conf. on Liquid Atomization and Spray Systems. Dearborn, Michigan, USA.*

Soteriou, C., Lambert, M., Zuelch, S. & Passerel, D. 2006. The flow characteristics of high efficiency Diesel nozzles with enhanced geometry holes. *Proc. THIESEL Intl Conf. on Thermo- and Fluid Dynamic Processes in Diesel Engines. Valencia, Spain.*

Vaidyanathan, R., Senocak, I., WU, J. Y. & Shyy, W. 2003. Sensitivity evaluation of a transport-based turbulent cavitation model. *Trans ASME J. Fluids Engng* **125**, 447–458.

Yakhot, V., Orszag, S. A., Thangam, S., Gatski, T. B. & Speziale, C. G. 1992. Development of turbulence models for shear flows by a double expansion technique. *Phy. Fluids* A **4**, 1510–1520.